

Characterization of high-frequency interconnects: Comparison between time- and frequency-domain methods

Mark Bieler and Uwe Arz

Physikalisch-Technische Bundesanstalt, Bundesallee 100, D-38116 Braunschweig, Germany

Email: mark.bieler@ptb.de, uwe.arz@ptb.de

Abstract—A high-frequency interconnect consisting of coplanar and coaxial elements is characterized using time- and frequency domain methods. As frequency-domain technique we employ conventional vector network analysis, while as time-domain technique a recently developed laser-based vector network analyzer is used. For the first time, both methods are compared in the frequency range from 10 GHz to 110 GHz. We obtain good agreement in almost the entire frequency range. Our results pave the way towards mutual independent verification of time- and frequency-domain high-frequency measurement techniques.

I. INTRODUCTION

High-frequency devices are usually characterized in the frequency domain using electronic vector network analyzers (VNA) [1]. This measurement technique is being continuously enhanced. The extension of VNA measurements in coaxial and rectangular waveguide connectors to higher frequencies is part of a European collaborative research initiative [2]. Moreover, traceable frequency-domain VNA measurements for planar circuits are currently being developed within the new European project PlanarCal [3].

In addition to frequency-domain methods, also time-domain techniques can be employed for characterization of high-frequency devices. Especially the advent of femtosecond laser technology has boosted such methods, which have already been employed for the characterization of oscilloscopes [4], [5] or photodiodes [6]. Although laser-based optoelectronic techniques have an incredibly large bandwidth and are assumed to provide traceability to the SI, a detailed verification of traceability does not yet exist.

Recently, we have demonstrated a one-port laser-based optoelectronic VNA [7], where femtosecond laser pulses are used to measure voltage signals in the time-domain on a planar waveguide. The separation between forward and backward propagating signals, being the key task of VNAs, is realized by measuring voltage signals at different positions on the planar waveguide. With this improvement, which has been obtained within two European research projects [8], [9], laser-based techniques can now be used to perform vector network analysis considering every type of mismatch [7].

Here we characterize a complex interconnect consisting of coaxial and coplanar elements using both, laser-based and conventional VNAs. We measure the interconnects scattering parameter S_{12} with both methods and obtain good agreement

in the frequency range from 10 GHz to 110 GHz. Our study constitutes a successful first step for independent validation of time-domain and frequency-domain methods. In this regard we emphasize that the measured quantity for both techniques is very different. In the time-domain method we measure electric fields, while frequency-domain VNAs measure power waves.

II. DEVICE UNDER TEST

Our device under test (DUT) consists of several different elements and is pictured in Fig. 1. A 20-cm long semi-rigid cable is connected to a coaxial-coplanar microwave probe both having 1.0-mm coaxial connectors. The microwave probe is attached to a 2-mm long coplanar waveguide (CPW). Figure 2 shows the characteristic impedance of the CPW calculated using the model of [10]. While the end of the CPW constitutes port 1 with a characteristic impedance Z_{CPW} being complex at low frequencies (see Fig. 2), the end of the coaxial semi-rigid cable constitutes port 2 with a characteristic impedance taken as 50Ω . Our comparison will focus on the S_{12} scattering parameter, see also Fig. 1, with the characteristic port impedances as noted above, i.e., no impedance transformation is performed. We have chosen a rather complex DUT to demonstrate that the conclusions drawn from our comparison are applicable to both, coplanar and coaxial structures. However, as explained in the following section, some properties of the DUT also help us to simplify the analysis of the time-domain measurements.

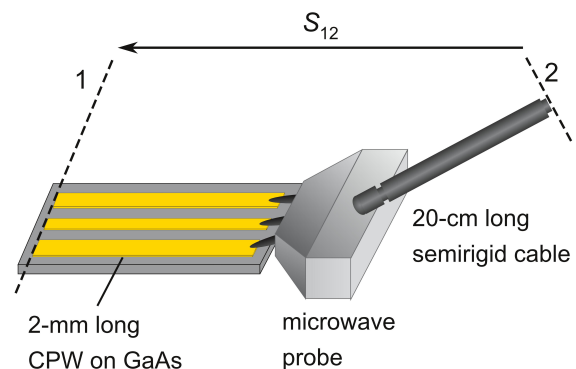


Fig. 1. Device under test and definition of scattering parameters.

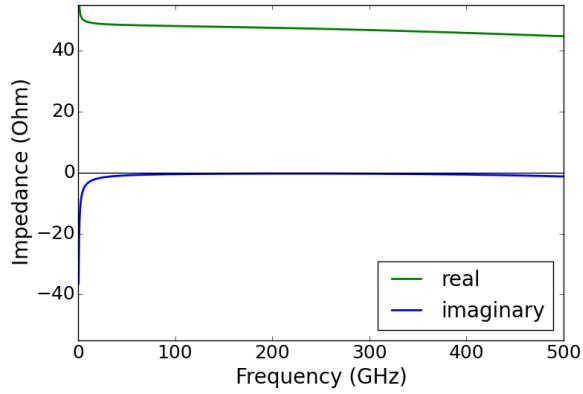


Fig. 2. Real and imaginary parts of the characteristic impedance of the CPW.

III. TIME-DOMAIN TECHNIQUE

The laser-based setup is shown in Fig. 3(a). Ultrashort voltage pulses are generated by focusing a laser beam (~ 350 -fs pulse width, ~ 800 -nm center wavelength, referred to as pump beam) onto a biased photoconductive gap, which is integrated into a 4-mm long CPW. The CPW is evaporated onto low-temperature-grown GaAs with a carrier life time of ~ 1 ps enabling the generation of very short voltage pulses. A second laser beam (~ 100 -fs pulse width, ~ 1600 -nm center wavelength, referred to as probe beam), which is synchronized to the first laser beam is used to measure the electric field of the voltage pulses by employing the electro-optic effect of the GaAs substrate and a typical electro-optic detection set-up. Here the measured signal is proportional to the electric field of the voltage pulses. By changing the time-delay between the pump and probe pulses with a motorized translation stage, the shape of the voltage pulse is electro-optically sampled. The translation stage is calibrated to the unit of time, providing traceability of the time axis of the voltage pulses.

Measurement of two voltage pulses V_1 and V_2 at different positions on the CPW allows for the separation of forward and backward propagating voltage signals [7]. This in turn enables us to calculate the complex reflection coefficient at the CPW measurement plane, which we place 2 mm away from the end of the CPW, from

$$\Gamma = \frac{V_2 - \mathbf{p}V_1}{\mathbf{p}(V_1 - \mathbf{p}V_2)} \mathbf{R} \quad (1)$$

with \mathbf{R} being a Tikhonov regularization filter to account for noise; \mathbf{p} is the transfer function of the CPW between the two measurement positions. The latter is obtained from parts of V_1 and V_2 which do not contain any reflections [7].

Attaching the microwave probe with the semi-rigid cable to the CPW, we obtain our DUT. If the coaxial end of the DUT is terminated with a short, \mathbf{R}_s , the reflection coefficient at the CPW measurement plane will be equal to:

$$\Gamma_{\text{CPW}} = \mathbf{S}_{11} + \frac{\mathbf{S}_{12}\mathbf{S}_{21}\mathbf{R}_s}{1 - \mathbf{R}_s\mathbf{S}_{22}} \quad (2)$$

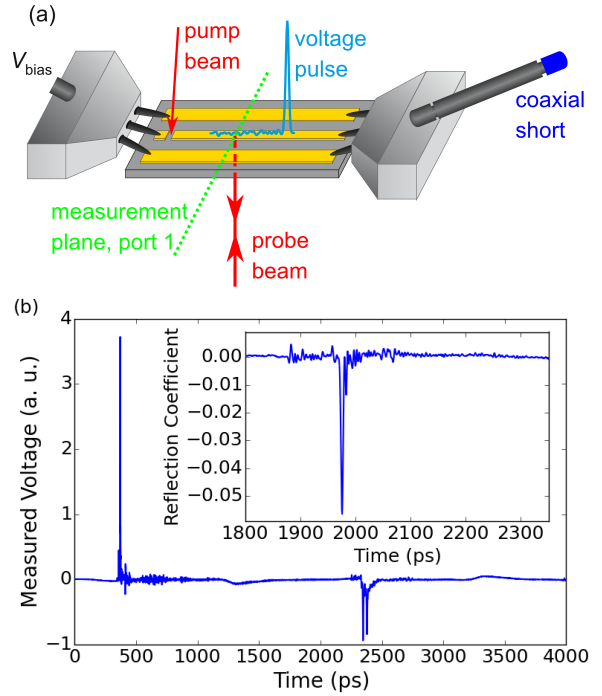


Fig. 3. (a) Setup for laser-based vector network analysis. (b) One of the two measured time-domain signals from which the scattering parameters were extracted. The inset shows a certain time window of the reflection coefficient at port 1.

Here Γ_{CPW} and \mathbf{S}_{11} are obtained from the two measured voltage pulses using (1). However, in contrast to Γ_{CPW} , \mathbf{S}_{11} is measured with the DUT not being terminated with the short but connected to another long semi-rigid cable, which, in turn, is terminated with a 50Ω load. This provides a perfect match of port 2, since any reflection from the 50Ω load does not reach the measurement plane within the measurement time window.

One of the measured voltage pulses obtained with the short being connected to the DUT is shown in Fig. 3(b). The measurement was performed over a time epoch of 4 ns with a 500-fs time step. Thus the trace consists of 8000 data points. While the signal at ~ 300 ps corresponds to the main voltage pulse traveling on the CPW towards the microwave probe, the signal at ~ 2300 ps corresponds to the voltage pulse being reflected from the short and reaching the CPW measurement plane again.

While it is not possible with our one-port laser-based VNA to measure \mathbf{S}_{22} precisely, its magnitude and phase influencing our measurements are estimated from the time-domain reflection coefficient shown in the inset of Fig. 3(b). The magnitude and phase of the short \mathbf{R}_s are obtained from finite element calculations [4]. After additionally considering the reciprocity relation

$$\frac{\mathbf{S}_{21}}{\mathbf{S}_{12}} = 1 - j \frac{\text{Im}(\mathbf{Z}_{\text{CPW}})}{\text{Re}(\mathbf{Z}_{\text{CPW}})} \quad (3)$$

as defined in [11], it is possible to solve (2) for \mathbf{S}_{12} .

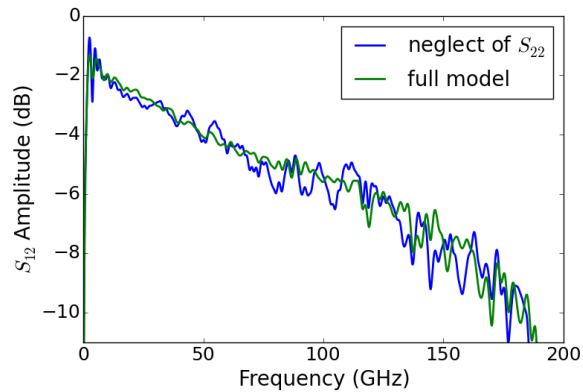


Fig. 4. Amplitude of S_{12} of the DUT obtained from the time-domain technique with and without considering S_{22} .

In Fig. 4 we plot the amplitude of S_{12} with and without considering S_{22} in (2). The neglect of S_{22} leads to severe oscillations. This is evidence of mismatch not being accurately eliminated. In contrast, accounting for S_{22} eliminates these oscillations.

The uncertainty analysis for the time-domain measurements is performed with Monte-Carlo simulations. In this analysis, the probability density functions of the input variables have either been obtained from repeated measurements or from other information.

IV. FREQUENCY-DOMAIN TECHNIQUE

For the frequency-domain measurement of S_{12} of our DUT we split up the DUT of Fig. 1 in two parts: the planar-coaxial part consisting of the 2-mm CPW length and the microwave probe, and the 20-cm semirigid cable part with coaxial 1.0-mm ports.

For characterizing the semirigid cable we first performed a two-port 1.0 mm calibration as recommended by the manufacturer of the broadband VNA system (Anritsu VectorStar). This calibration consists of a low-band and high-band part employing different calibration standards suitable for the respective band, which are merged afterwards to provide the bandwidth from 1 to 110 GHz used in this experiment.

For characterizing the planar-coaxial part, we utilized the two-port second-tier procedure described in [12]. To this end, two coplanar probes from the same manufacturer with the same GSG footprint were employed. We used the same two-port 1.0-mm calibration as in the semirigid cable characterization part to establish the coaxial reference plane at the coaxial ports. Then, we contacted coplanar waveguide artifacts of different lengths together with a reflect standard on the low-loss GaAs substrate. Using these measurements, we performed a second-tier Multiline-TRL calibration [13], moving the on-wafer reference plane into the middle of a 4-mm long coplanar waveguide.

Even though possible, we did not normalize the reference impedance at the on-wafer port to 50Ω . The characteristics

of the planar-coaxial part of the DUT were obtained as error boxes from the second-tier calibration.

For calculating the uncertainty of the frequency-domain measurement we used the NIST Microwave Uncertainty Framework [14], which implements both linear propagation of uncertainty and Monte Carlo simulations as uncertainty calculation methods. The uncertainties for the planar part of the DUT were calculated following the methodology outlined in [15].

V. DISCUSSION AND CONCLUSION

The amplitude of our DUTs S_{12} parameter obtained from both the time- and frequency domain methods are shown in Fig. 5. With the conventional VNA we obtain data up to 110 GHz limited by the coaxial 1.0-mm calibration kit definitions provided by the manufacturer. The effective bandwidth of the time-domain VNA is mainly limited by the width of the ultrashort voltage pulses. We typically obtain spectral components >500 GHz [7]. Below 10 GHz the uncertainty of the time-domain result is very large. This is mainly due to the measurement over limited time windows and the subsequent data analysis. Therefore we only compare the range from 10 GHz to 110 GHz. We obtain a good agreement between both techniques, although the 95% confidence intervals do not overlap at every frequency point. In this regard we emphasize two things: (i) The model from which the time-domain results were extracted is not perfect and might contain small systematic errors. (ii) The uncertainty analysis for the frequency-domain measurements is still under development [2,3]. We believe that this might explain the differences at certain frequencies between the time- and frequency-domain results. In any case we take our results as a first encouraging step towards mutual verification of time- and frequency-domain high-frequency device characterization. Comparisons on additional high-frequency elements and an improvement of the time-domain method will be in the focus of future studies.

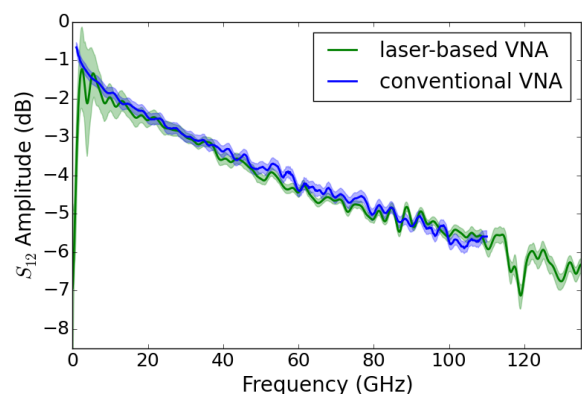


Fig. 5. Amplitude of S_{12} of the DUT obtained from the time- and frequency-domain techniques (thick lines). The 95% confidence intervals are marked by the light semi-transparent colors.

ACKNOWLEDGMENT

The authors acknowledge support by the European Metrology Research Programme (EMRP) and the European Metrology Programme for Innovation and Research (EMPIR). The EMRP programme is jointly funded by the EMRP participating countries within EURAMET and the European Union. The EMPIR programme is co-financed by the Participating States and from the European Union's Horizon 2020 research and innovation programme. The authors also thank D. Schubert, K. Pierz, H. Marx, and B. Hacke for expert technical assistance.

REFERENCES

- [1] D. Rytting, "An Analysis of Vector Measurement Accuracy Enhancement Techniques," *Hewlett-Packard RF & Microwave Measurement Symposium and Exhibition*, 1982.
- [2] Metrology for new electrical measurement quantities in high-frequency circuits. European Metrology Research Programme JRP Number SIB62. [Online]. Available: <http://projects.npl.co.uk/hf-circuits>
- [3] Microwave measurements for planar circuits and components. European Metrology Programme for Innovation and Research JRP Number IND02. [Online]. Available: <http://planarcal.ptb.de>
- [4] H. Füser, S. Eichstädt, K. Baaske, C. Elster, K. Kuhlmann, R. Judaschke, K. Pierz, and M. Bieler, "Optoelectronic Time-Domain Characterization of a 100 GHz Sampling Oscilloscope," *Measurement Science and Technology*, vol. 23, no. 2, p. 025201, Feb. 2012.
- [5] M. Harper, A. Smith, A. Basu, and D. Humphreys, "Calibration of a 70 GHz Oscilloscope," in *CPEM Digest, 2004*, 2004, pp. 530–531.
- [6] D. Williams, A. Lewandowski, T. Clement, J. Wang, P. Hale, J. Morgan, D. Keenan, and A. Dienstfrey, "Covariance-Based Uncertainty Analysis of the NIST Electrooptic Sampling System," *IEEE Trans. Microw. Theory Tech.*, vol. 54, pp. 481–491, Jan. 2006.
- [7] M. Bieler, H. Füser, and K. Pierz, "Time-Domain Optoelectronic Vector Network Analysis on Coplanar Waveguides," *IEEE Transactions on Microwave Theory and Techniques*, vol. 63, no. 11, pp. 3775–3784, Nov. 2015.
- [8] Metrology for ultrafast electronics and high-speed communications. European Metrology Research Programme JRP Number IND16. [Online]. Available: <http://www.ptb.de/emrp/ultrafast.html>
- [9] Metrology for optical and rf communication systems. European Metrology Research Programme JRP Number IND51. [Online]. Available: <http://www.emrp-ind51-morse.org>
- [10] F. Schnieder, T. Tischler, and W. Heinrich, "Modeling Dispersion and Radiation Characteristics of Conductor-Backed CPW With Finite Ground Width," *IEEE Trans. Microwave Theory and Techniques*, vol. 51, no. 1, pp. 137–143, Jan. 2003.
- [11] Roger B. Marks and Dylan F. Williams, "A General Waveguide Circuit Theory," *J. Res. Natl. Inst. Stand. Technol.*, vol. 97, no. 5, pp. 533–562, Oct. 1992.
- [12] U. Arz and D. Schubert, "Coplanar Microwave Probe Characterization: Caveats and Pitfalls," in *67th ARFTG Microwave Measurements Conference*, Jun. 2006, pp. 214–218.
- [13] Roger B. Marks, "A Multiline Method of Network Analyzer Calibration," *IEEE Trans. Microwave Theory and Techniques*, vol. 35, no. 7, pp. 1205–1215, Jul. 1991.
- [14] NIST Microwave Uncertainty Framework, Beta Version. [Online]. Available: <http://www.nist.gov/ctl/rf-technology/related-software.cfm>
- [15] U. Arz and D.F. Williams, "Uncertainties in complex permittivity extraction from coplanar waveguide scattering-parameter data," in *81st ARFTG Microwave Measurements Conference*, Jun. 2013, pp. 120–125.